

MACHINE LEARNING ALGORITHM FOR AUTOMATIC DETECTION OF CT-IDENTIFIABLE HYPERDENSE LESIONS ASSOCIATED WITH TRAUMATIC BRAIN INJURY

Krishna N. Keshavamurthy^{(1),a}, Owen P. Leary^{a,c}, Lisa H. Merck^{b,c}, Benjamin Kimia^a, Scott Collins^c, David W. Wright^d, Jason W. Allen^e, Jeffrey F. Brock^f, Derek Merck^{a,c}

^aDept. of Engineering, Brown University, 182 Hope Street, Providence, RI, USA 02912

^bDept. of Emergency Medicine, The Warren Alpert Medical School of Brown University, 222 Richmond Street, Providence, RI, USA 02903

^cDept. of Diagnostic Imaging, Rhode Island Hospital, 293 Eddy Street, Providence, RI, USA, 02903

^dDept. of Emergency Medicine, Emory University School of Medicine, 1648 Pierce Drive NE, Atlanta, GA, 30307

^eDept. of Radiology, Emory University School of Medicine, 1648 Pierce Drive NE, Atlanta, GA, 30307

^fDept. of Mathematics, Brown University, Box 1917, Providence, RI, USA 02912

ABSTRACT

Traumatic brain injury (TBI) is a major cause of death and disability in the United States. Time to treatment is often related to patient outcome. Access to cerebral imaging data in a timely manner is a vital component of patient care. Current methods of detecting and quantifying intracranial pathology can be time-consuming and require careful review of 2D/3D patient images by a radiologist. Additional time is needed for image protocoling, acquisition, and processing. These steps often occur in series, adding more time to the process and potentially delaying time-dependent management decisions for patients with traumatic brain injury.

Our team adapted machine learning and computer vision methods to develop a technique that rapidly and automatically detects CT-identifiable lesions. Specifically, we use scale invariant feature transform (SIFT)¹ and deep convolutional neural networks (CNN)² to identify important image features that can distinguish TBI lesions from background data. Our learning algorithm is a linear support vector machine (SVM)³. Further, we also employ tools from topological data analysis (TDA) for gleaning insights into the correlation patterns between healthy and pathological data. The technique was validated using 409 CT scans of the brain, acquired via the Progesterone for the Treatment of Traumatic Brain Injury phase III clinical trial (ProTECT_III) which studied patients with moderate to severe TBI⁴. CT data were annotated by a central radiologist and included patients with positive and negative scans. Additionally, the largest lesion on each positive scan was manually segmented. We reserved 80% of the data for training the SVM and used the remaining 20% for testing. Preliminary results are promising with 92.55% prediction accuracy (sensitivity = 91.15%, specificity = 93.45%), indicating the potential usefulness of this technique in clinical scenarios.

Keywords: Traumatic Brain Injury (TBI), Scale Invariant Feature Transform (SIFT), Convolutional Neural Networks (CNN), Computed Tomography (CT), Machine Learning, Support Vector Machine, Lesion Detector

1. INTRODUCTION

In the United States, traumatic brain injury (TBI) is responsible for disability in 5.3 million people, 2.8 million emergency department visits per year, and one third of all trauma-related mortality⁵. TBI diagnosis and severity classification are commonly evaluated via mechanism of injury, brain function (Glasgow Coma Score), and medical imaging^{6,7}. Severe TBI is often complicated by intracranial hemorrhage⁸. Such hemorrhages can be dynamic and expand over time, worsening injury^{9,10}. Clinical experience has shown that prompt treatment of patients with severe TBI is directly related to improved patient outcome^{11,12}.

Neuroimaging is often instrumental in confirming the presence of brain trauma soon after a patient arrives at the emergency department. Qualities of brain hemorrhage identified on neuroimaging, such as estimated lesion volume and

¹ (1) krishna_nand_keshava_murthy@brown.edu

location, are considered valuable data for prognostication and patient management¹³⁻¹⁵. In patients arriving at the emergency department within 24 hours of injury, and for whom neuroimaging is indicated, computed tomography (CT) is usually considered the first choice for assessing suspected TBI¹⁶⁻¹⁸. Advances in image processing and diagnostics will reduce time to treatment after TBI and improve survival.

Interpretation of brain CT images is most often dependent on the availability of a neuro-radiologist. While their expertise is advantageous, a process that can rapidly and automatically provide information regarding the need for emergent intervention – such as an expanding hematoma, would provide added value to the emergency care team. Moreover, the current techniques used by most radiologists to estimate hemorrhage volume from imaging data may be inaccurate, especially for large and more irregularly-shaped lesions^{19,20}. Significant discrepancy has also been shown between the clinical interpretation of head CT by emergency medicine teams and by more specialized neuroradiologists, suggesting some level of inconsistency in CT interpretation across providers²¹. Even among neuroradiologists, statistically significant differences in interpretation have been shown^{22,23}, though the clinical impact of these differences might be slight²⁴. There is also an inevitable delay in patient care caused by waiting for the scan to be reviewed. Such concerns motivate a more efficient method of identifying brain pathology from CT while maintaining or improving accuracy.

A potential solution is an automatic TBI detection tool that can accurately identify hemorrhage presence and volume from CT data in terms of injury severity and lesion characteristics. There have been several previous studies that attempt to automatically detect TBI characteristics^{25,26} as well as predict TBI severity score and intracranial pressure. Other research has demonstrated the viability of various machine learning approaches to detecting or delineating ischemic and hemorrhagic lesions in CT data²⁷⁻³⁰. However, these studies have been conducted on relatively small data sets (with 62 or fewer manually segmented positive cases), and performance of these methods on larger CT data sets has not been thoroughly explored. There have also been several attempts at automated segmentation and classification of hemorrhagic lesions or tumors from magnetic resonance (MR) data³¹⁻³⁸. Recent results from MR have been promising, but MR is not readily available in most trauma centers and is more expensive.

In this work, we propose a machine learning approach to rapidly and automatically detect the presence of hyperdense regions indicative of brain hemorrhage in a large (n=409) CT data set. With the motivation that the TBI lesions differ from healthy tissue in their intensity characteristics on CT, we employ the scale-invariant feature transform (SIFT) and convolutional neural networks (CNN) for extracting intensity features. We then train a linear SVM for automatically detecting TBI lesion in CT. The two different features are compared in terms of accuracy, sensitivity, and specificity of classification performance. Further, we employ novel tools from topological data analysis to examine the topological characteristics of our data set and derive conclusions that confirm our SVM results. Our methodologies could be implemented in parallel with standard image processing to precede diagnostic interpretation by the radiologist. Findings which are potentially of concern would be flagged for immediate review by the physician specialist, leading to a reduction in the time to identify and treat intracranial pathology detected on brain imaging.

2. METHODS

Data

The CT volumes used in this study were collected during the ProTECTIII phase 3 multicenter clinical trial designed to test the efficacy of intravenous progesterone on patient outcome following moderate to severe TBI⁴. All DICOM data used in this study were captured within four hours of injury and subsequently anonymized. The initial slice thickness of these data ranges from 1.5 to 5 mm. Imaging reveals the contrast between high-density regions representing localized intracranial hemorrhage and normal density regions representing non-pathological brain tissue. A heterogeneous cross-section of hemorrhage types is represented in this data set. Each case was individually examined by a central neuroradiologist as part of the ProTECTIII trial and marked as positive or negative for TBI-related pathology.

Of the 882 baseline scans, 409 were chosen for this study. Each selected image that was marked positive underwent advanced image analysis via manual segmentation by a trained research assistant under the supervision of physicians in diagnostic imaging. The largest lesion in each positive case was segmented using *3D Slicer*³⁹, as seen in figure 1, after the data were normalized through resampling. Of the 409 cases in our study, 222 cases featured visible lesions and the remaining 187 cases did not feature visible lesions on initial CT imaging. 80% of the cases were randomly selected for training the machine learning algorithm, and the remaining 20% of cases were used for testing the algorithm. As our

ground truth, each CT slice was labeled as positive if it contained a pathological lesion identified by the neuroradiologist and via manual segmentation. CT slices from cases identified as negative for visible pathology by the neuroradiologist, were labeled as negative, and did not undergo resampling.

This data set was subjected to rigorous physiologic monitoring of subjects and documentation of patient outcomes, potentially of interest to future studies. In addition to the baseline scans used in this study, the larger data set includes over 2200 follow-up scans captured at regular time intervals post-injury. The volumetric resampling and illustration protocol developed as part of this study (which will eventually be applied to all of the scans of the data set) was as follows: first, thick-slice positive CT volumes were re-thinned to a uniform slice thickness of 1.5mm and symmetrized about the midsagittal plane of the brain, both using *Aquarius (TeraRecon Inc, 2012)*. The largest lesion in each positive case, identified by the neuroradiologist, was then traced by hand on each CT slice using *3D Slicer (v.4.5)*, producing ground truth lesion labels for all volumes positive for pathology. The resulting processed data is a well-curated set of valuable clinical and volumetric information that was uniformly collected for ease of comparison.

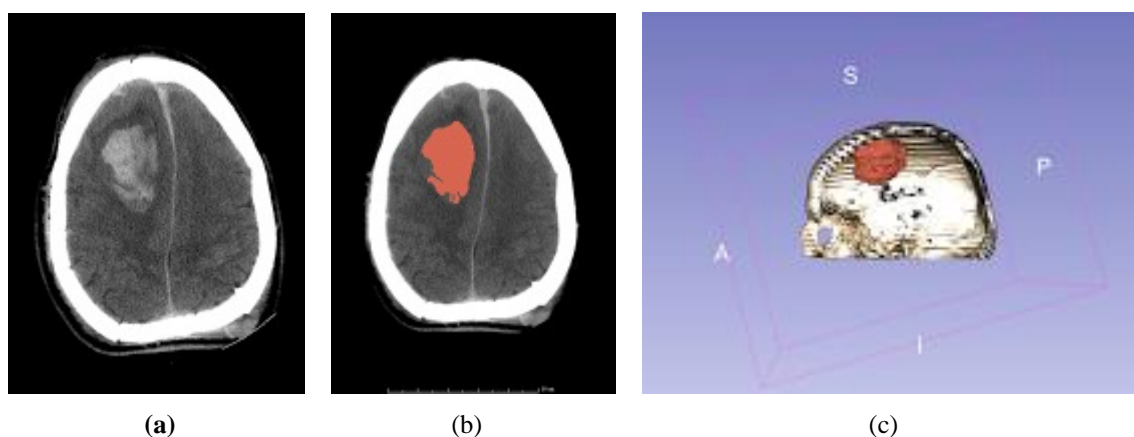


Figure 1. Semi-automated 3D Illustration: (a) Axial computed tomography (CT) image containing a hyperdense region representing a traumatic intraparenchymal hemorrhage (IPH) located in the right frontal lobe (b) The same CT image, in which the lesion has been traced and labelled using *3D Slicer* (c) Three-dimensional rendering of the same IPH generated using *3D Slicer*, oriented within the DICOM volume of the patient's skull; the letters A, S, P, and I correspond with anatomical directions about the patient's skull (anterior, superior, posterior, and inferior, respectively).

Methodology

Given CT slices from all the training cases with positive (with lesion) and negative (no lesion) ground truth annotations, our goal was to predict whether new slices contained a lesion. Further, using the slice predictions, we wanted to predict whether a new case (i.e. a whole CT volume) contains pathology. We divide our prediction methodology into two stages: feature extraction and machine learning algorithm, as explained below. We then briefly describe the topological data analysis methodology.

2.1.1 Feature Extraction

Feature extraction is one of the key components in computer vision. In this study, one of the goals was to identify the right image features that can help distinguish between pathological and healthy brain tissue. We observed that lesion-containing regions differ from normal brain tissue in their CT intensity (Hounsfield) pattern (see figures 1(a) and 1(b)). We also observed that the lesion detector should be invariant to scale (i.e. independent of the size of the lesion), invariant to rotation, and invariant to translation (i.e. independent of the specific orientation or location of the lesion). With these conditions in mind, we employed two different types of image features: SIFT¹ and CNN². Below, we briefly describe how the features are computed.

SIFT features are computed by first extracting key points in the CT slices that are local extrema of the difference of Gaussian filter response across space and scales. The characteristic scale of the key point and the dominant gradient

direction (in the neighborhood of the key point) are assigned to each key point. Then SIFT descriptors are computed at all the key points by concatenating histograms of image gradient orientations around each key point. Each SIFT descriptor is a 128-dimensional vector encoding the local image intensity gradient orientation information. To represent each CT slice using SIFT features, we use the bag of visual words model for images⁴⁰. We first pool all SIFT descriptors from all the training slices, gathered from the training cases, and vector quantize them using the K-means clustering algorithm. This gives us K cluster centers, each of which is a 128-dimensional vector. Then for each CT slice, we assign its SIFT features to their closest cluster centers and build a histogram of the SIFT features assigned to each of the clusters. This histogram is further normalized such that it adds to 1. This K dimensional histogram is our final representation for each CT slice.

A CNN is a multi-layered artificial neural network with alternating convolutional and pooling filters in its different layers. The CNN is trained by minimizing the loss function that penalizes the deviation between the predicted and true labels using the back propagation algorithm. In this work, we used the AlexNet, which is a network with 5 convolutional layers and 3 fully connected layers⁴¹. As a first step towards employing CNNs in our work, we experimented using the network weights pre-trained on the ImageNet (natural images) data set⁴². Each CT slice was then fed independently into this network and the output of the first fully connected layer was used as the feature vector for the slice.

2.1.2 Machine Learning Algorithm

Our machine learning algorithm is a linear SVM³. The SVM objective function consists of the average hinge loss to measure data fidelity and the norm of the weight vector to impose regularization. This convex objective function was minimized using the stochastic gradient descent algorithm to find the optimal hyperplane that separates the positive (with lesion) from the negative (no lesion) CT slices in the training data. We classified our testing data (slices from the testing cases) as positive or negative and computed our prediction accuracy by comparing them with the ground truth slice annotations. Furthermore, to incorporate the observation that lesions always appear on CT slices that are contiguous, we use a simple neighborhood voting rule to decide if a slice prediction is to be retained. If both the above and below neighbor slice predictions match, then the prediction of the slice under consideration is also set to match its neighbor predictions. To transition from slice based prediction to case based prediction, we predict the whole case as positive if its CT scan has at least 6 mm of lesion in the axial dimension. This criterion is based on the estimation that the smallest segmented lesion visible in our data set was approximately 6 mm in the axial dimension.

2.1.3 Topological Data Analysis

Recently, techniques from the fields of algebraic topology and the study of large finite metric spaces have led to novel applications in analyzing the topological properties of data. This field of study, called *topological data analysis* (TDA)⁴³, enables us to understand the “shape” of the data, i.e. how the data clusters (patterns of correlation), and if there are structures that correlate with certain characteristics, e.g. clinical outcomes. Here, we apply TDA methodologies to glean insights into the correlation patterns among healthy and pathological CT slices. Specifically, we use the Ayasdi software^{44,45} to build the so called simplicial complex representation of the SIFT visual word histogram data obtained above from CT slices. This involves first choosing a function called the *lens function*, which transforms the data to a lower dimensional space. Then the co-domain of the lens function is divided into overlapping intervals, whose domains are further clustered using a chosen distance metric in the original data (SIFT visual word histograms in our case) space. Clusters that have common data points are connected through links. The obtained connectivity pattern is visualized by 2D projection onto the computer screen.

3. RESULTS

For all our experiments, we used MATLAB⁴⁶ software for all computations. We used the vlfeat library⁴⁷ for both SIFT feature extraction and SVM training. The value of K for computing the bag of visual words was empirically set to 200. To set the regularization parameter for the SVM, we used 10-fold cross validation. For computing the CNN features, we used the MatConvNet² MATLAB library. We extracted the output of the first fully connected layer, a 4096 length vector, as the feature for each CT slice. For TDA computations and visualization, we used the Ayasdi software.

We evaluated the classification performance of the SVM in terms of accuracy, sensitivity, and specificity for both SIFT and CNN. Table 1 shows our results. The top half of the table shows the slice based prediction performance, i.e. the

ability of the SVM to predict the presence of traumatic lesions on slices of CT data. The bottom half of the table shows the case based prediction performance, i.e. the ability of the SVM to predict the presence of traumatic lesion in volumes of CT data (whole cases).

	Accuracy	Sensitivity	Specificity
Feature	Slice Prediction Performance (Positive or Negative)		
<i>SIFT</i>	92.55%	91.15%	93.45%
<i>CNN</i>	90.50%	93.96%	88.29%
	Case Prediction Performance (Positive or Negative)		
<i>SIFT</i>	90.00%	100.00%	79.00%
<i>CNN</i>	82.50%	100.00%	62.00%

Table 1: Classifier performance measures. Both slice (2D) and case (3D) prediction results were averaged over 500 runs of the SVM.

As we can see, the SVM achieves high classification performance across the board for both slice as well as case based prediction. In particular, we note that the SIFT features outperform the CNN features. But we wish to remind here that the CNN was pre-trained on the ImageNet data. We expect the CNN performance to improve with fine-tuned training on our data. Our results for SIFT performance on 2D slice classification were further investigated through ROC curve analysis (figure 2). As we observe, we achieve a high area under the curve (AUC) and low equal error rate (EER).

Next, we present results of topological data analysis using Ayasdi software. For the lens function, we used the neighborhood lens, which is based on embedding a nearest neighbor graph in 2D Euclidean space. For clustering, we used variance normalized Euclidean distance as the metric. Figure 3 shows the 2D visualization of the simplicial complex using Ayasdi's algorithm. Nodes in the network represent clusters of bag of visual word histogram features from CT slices and edges connect nodes that contain features in common. We want to point out that the actual position of the nodes or the length of the edges themselves don't carry any information. The nodes are colored red for pathological slices and green for healthy slices. As we can see, the nodes from pathological slices are densely connected to each other and so are nodes from healthy slices. This shows that the pathological slices are more similar to each other than to healthy slices and vice-versa. We also observe that the pathological and healthy slices form separable clusters in the topological space, confirming our SVM results. Some of the nodes have intermediate coloration (neither green nor red), like orange, since those nodes have a mix of healthy as well as pathological slices. There is additional information contained in the TDA diagram, including loops as well as several outlying nodes, whose analysis will be part of our future work.

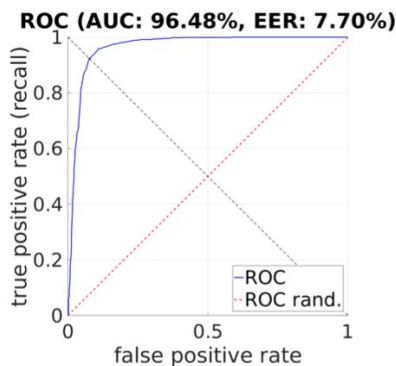


Figure 2. ROC Curve Analysis: We see that the classifier achieves very high area under the curve and very low equal error rate.

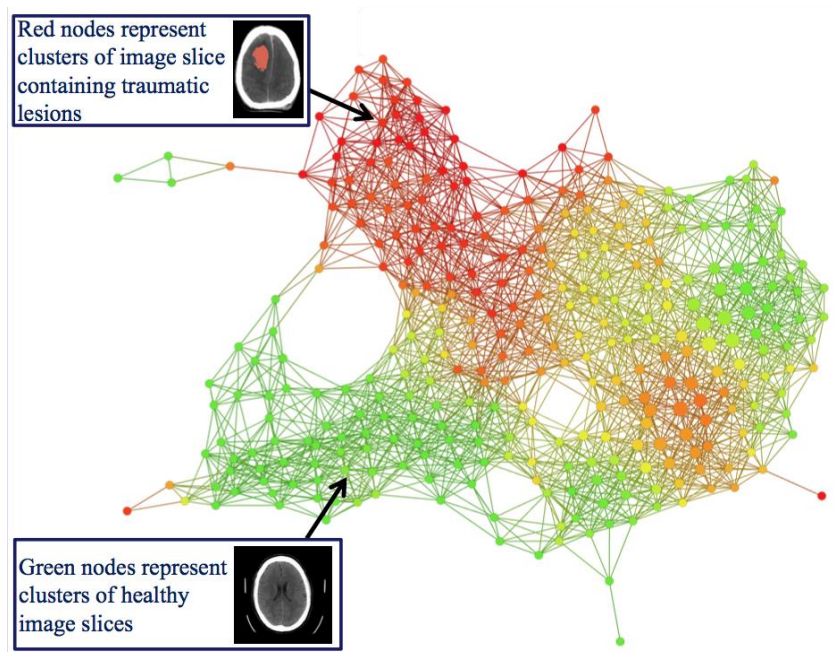


Figure 3. Topological Data Analysis (TDA): Analyzing the topological structure of the data, in which nodes represent clusters of bag of visual word histogram features from image slices. The edges connect nodes that contain features in common. The nodes are colored red for pathological slices and green for healthy slices. As we can see, the pathological and healthy slices are densely connected among themselves and form separable clusters in the topological space, confirming our SVM results.

4. CONCLUSIONS AND FUTURE WORK

We present a machine learning approach for detecting the presence of hyperdense lesions in CT data, both in individual slices and entire cases, and demonstrate high accuracy, specificity, and selectivity. To our knowledge, this study is the first successful use of a data set of this size for automatic detection of lesions due to TBI. As we notice in the results, SIFT performs better than the CNN features. This could be due in part to our use of the ImageNET pre-trained CNN network. We also applied topological data analysis methodologies and presented visualizations of patterns of correlation among healthy and pathological CT slices. These tools further confirm our SVM results. Future work will involve

training a CNN on our CT data from scratch, which might improve the performance of the CNN, resulting in more accurate predictions. We also plan to incorporate the slice neighborhood constraints and spatial constraints more rigorously using probabilistic graphical models and extend our algorithm to automatically segment the lesions in the data set. Finally, we plan to investigate the topological properties of the data and their relationship with patient outcomes more deeply using TDA methodologies like persistent homology.

REFERENCES

- [1] Lowe, D.G., “Distinctive image features from scale-invariant keypoints,” *Int J Computer Vision* **60**(2), 91-110 (Nov 2004).
- [2] Vedaldi, A., and Lenc, K., “MatConvNet – Convolutional neural networks for MATLAB,” *Proc ACM Int Conf on Multimedia* **2015**, (2015).
- [3] Fan, R., Chang, K., Hsieh, C., Wang, X., and Lin, C., “LIBLINEAR: A library for large linear classification,” *J Machine Learning Res* **9**, 1871-1874 (Jun 2007).
- [4] Wright, D.W., Yeatts, S.D., Silbergleit, R., Palesch, Y.Y., Hertzberg, V.S., Frankel, M., Goldstein, F.C., Caveney, A.F., Howlett-Smith, H., Bengelink, E.M., Manley, G.T., Merck, L.H., Janis, L.S., Barsan, W.G., and NETT Investigators, “Very early administration of progesterone for acute traumatic brain injury,” *N Engl J Med* **371**(26), 2457-2466 (2014).
- [5] Taylor, C.A., Bell, J.M., Breiding, M.J., and Likang, X., “Traumatic brain injury-related emergency department visits, hospitalizations and deaths – United States, 2007 and 2013,” *MMWR Surveill Summ* **66**(9), 1-16 (Mar 2017).
- [6] Maas, A.I.R., Stocchetti, N., and Bullock, R., “Moderate and severe traumatic brain injury in adults,” *The Lancet Neurology* **7**(8), 728-741 (2008).
- [7] Jennett, B., “The Glasgow coma scale: history and current practice,” *Trauma* **4**, 91-103 (2002).
- [8] Kazui, S., Naritomi, H., Yamamoto, H., Sawada, T., and Yamaguchi, T., “Enlargement of spontaneous intracerebral hemorrhage: incidence and time course,” *Stroke* **27**, 1783-1787 (1996).
- [9] Oertel, M., Kelly, D.F., McArthur, D., Boscardin, W.J., Glenn, T.C., Lee, J.H., Gravori, T., Obukhov, D., McBride, D.Q., and Martin, N.A., “Progressive hemorrhage after head trauma: predictors and consequences of evolving injury,” *J Neurosurgery* **96**, 109-116 (2002).
- [10] Stein, S.C., Spettell, C., Young, G.M.A., and Ross, S.E., “Delayed and progressive brain injury in closed-head trauma: radiological demonstration,” *Neurosurgery* **32**(1), 25-31 (1993).
- [11] Tepas, J.J., Leaphard, C.L., Pieper, P., Beaulieu, C.L., Spierre, L.R., Tuten, J.D., and Celso, B.G., “The effect of delay in rehabilitation on outcome of severe traumatic brain injury,” *J Pediatric Surgery* **44**(2), 368-72 (2009).
- [12] Dinh, M.M., Bein, K., Roncal, S., Byrne, C.M., Petchell, J., and Brennan, J., “Redefining the golden hour for severe head injury in an urban setting: the effect of prehospital arrival times on patient outcomes,” *Injury* **44**, 606-610 (2013).
- [13] Poon, M.T., Fonville, A.F., and Al-Shahi Salman, R., “Long-term prognosis after intracerebral hemorrhage: systematic review and meta-analysis,” *J Neurol Neurosurg Psychiatry* **85**(6), 660-667 (2014).
- [14] Broderick, J.P., Brott, T.G., Duldner, J.E., Tomsick, T., and Huster, G., “Volume of intracerebral hemorrhage. A powerful and easy-to-use predictor of 30-day mortality,” *Stroke* **24**(7), 987-993 (Jul 1993).
- [15] Bullock, M.R., Chesnut, R., Ghajar, J., Gordon, D., Hartl, R., Newell, D.W., Servadei, F., Walters, B.C., Wilberger, J., and Surgical Management of Traumatic Brain Injury Author Group, “Surgical management of traumatic parenchymal lesions,” *Neurosurgery* **58**(3), S25-S46 (Mar 2006).
- [16] Lee, B., Newberg, A., “Neuroimaging in traumatic brain injury,” *NeuroRx* **2**(2), 372-383 (Apr 2005).
- [17] Kelly, A.B., Zimmerman, R.D., Snow, R.B., Gandy, S.E., Heier, L.A., and Deck, M.D., “Head trauma: comparison of MR and CT – experience in 100 patients,” *Am J Neuroradiol* **9**(4), 699-708 (1988).
- [18] Glauser, J., “Head injury: Which patients need imaging? Which test is best?” *Cleveland Clinic J of Medicine* **71**(4), 353-357 (2004).
- [19] Hussein, H.M., Tariq, N.A., Palesch, Y.Y., Qureshi, A.I., and ATACH Investigators, “Reliability of hematoma volume measurement at local sites in a multicenter acute intracerebral hemorrhage clinical trial,” *Stroke* **44**, 237-239 (2013).
- [20] Webb, A.J.S., Ullman, N.L., Morgan, T.C., Muschelli, J., Kornbluth, J., Awad, I.A., Mayo, S., Rosenblum, M., Ziai, W., Zuccarello, M., Aldrich, F., John, S., Harnof, S., Lopez, G., Broaddus, W.C., Wijman, C., Vespa, P., Bullock, R., Haines, S.J., Cruz-Flores, S., Tuhim, S., Hill, M.D., Narayan, R., and Hanley, D.F., “Accuracy of the ABC/2 score for

intracerebral hemorrhage: systematic review and analysis of MISTIE, CLEAR-IVH, CLEAR III,” *Stroke* **46**, 2470-2476 (2015).

- [21] Talebian, M., Kavandi, E., Farahmand, S., Shahlafar, N., Arbab, M., Seyedhosseini-Davarani, S., Nejati, A., and Bagheri-Hariri, S., “Comparing the brain CT scan interpretation of emergency medicine team with radiologists’ report and its impact on patient outcome,” *Emergency Radiology* **22**, 261-268 (2015).
- [22] Viertel, V.G., Babiarz, L.S., Carone, M., Lewin, J.S., and Yousem, D.M., “Quality control in neuroradiology: impact of trainees on discrepancy rates,” *Am J Neuroradiol* **33**, 1032-1036 (2012).
- [23] Babiarz, L.S., and Yousem, D.M., “Quality control in neuroradiology: discrepancies in image interpretation among academic neuroradiologists,” *Am J Neuroradiol* **33**, 37-42 (2012).
- [24] Lal, N.R., Murray, U.M., Eldevik, O.P., and Desmond, J.S., “Clinical consequences of misinterpretations of neuroradiologic CT scans by on-call radiology residents,” *Am J Neuroradiol* **21**, 124-129 (2000).
- [25] Chong, S.L., Liu, N., Barbier, S., and Ong, M.E.H., “Predictive modeling in pediatric traumatic brain injury using machine learning,” *BMC Medical Res Methodol* **15**(22), (Mar 2015).
- [26] Chen, W., Cockrell, C., Ward, K.R., and Najaran, K., “Intracranial pressure level prediction in traumatic brain injury by extracting features from multiple sources and using machine learning methods,” *Proc IEEE Int Conf Bioinformatics Biomedicine* **2010**, 510-515 (Dec 2010).
- [27] Chan, T., “Computer aided detection of small acute intracranial hemorrhage on computer tomography of brain,” *Computerized Medical Imaging and Graphics* **31**, 285-298 (2007).
- [28] Maduskar, P., and Acharyya, M., “Automatic identification of intracranial hemorrhage in non-contrast CT with large slice thickness for trauma cases,” *Conf Proc SPIE Medical Imaging* **2009**, (Mar 2009).
- [29] Al-Ayyoub, M., Alawad, D., Al-Darabsah, K., and Aljarrah, I., “Automatic detection and classification of brain hemorrhages,” *WSEAS Trans on Computers* **10**(12), 395-405 (2013).
- [30] Gillebert, C.R., Humphreys, G.W., and Mantini, D., “Automated delineation of stroke lesions using brain CT images,” *Neuroimage: Clinical* **4**, 540-548 (Mar 2014).
- [31] Khotanlou, H., Colliot, O., Atif, J., and Block, I., “3D brain tumor segmentation in MRI using fuzzy classification, symmetry analysis and spatially constrained deformable models,” *Fuzzy Sets and Systems* **160**, 1457-1473 (2009).
- [32] Kharrat, A., Messaoud, M.B., Benamrane, N., and Abid, M., “Detection of brain tumor in medical images,” *Int Conf Signals Circuits Systems* **2009**, 1-6 (Nov 2009).
- [33] Juang, L., and Wu, M., “MRI brain lesion image detection based on color-converted K-means clustering segmentation,” *Measurement* **43**, 941-949 (2010).
- [34] Roy, S., Nag, S., Bandyopadhyay, S.K., Bhattacharyya, D., and Kim, T., “Automated brain hemorrhage lesion segmentation and classification from MR image using an innovative composite method,” *J Theoretical Applied Information Technology* **78**(1), 34-45 (2015).
- [35] Mitra, J., Shen, K., Ghose, S., Bourgeat, P., Frripp, J., Salvado, O., Pannek, K., Taylor, D.J., Mathias, J.L., and Rose, S., “Statistical machine learning to identify traumatic brain injury (TBI) from structural disconnections of white matter networks,” *NeuroImage* **129**, 247-259 (2016).
- [36] Kamnitsas, K., Ledig, C., Newcombe, V.F.J., Simpson, J.P., Kane, A.D., Menon, D.K., Rueckert, D., and Glocker, B., “Efficient multi-scale 3D CNN with fully connected CRF for accurate brain lesion segmentation,” *Medical Image Analysis* **36**, 61-78 (Feb 2017).
- [37] Vergara, V.M., Mayer, A.R., Damaraju, E., Keihl, K.A., and Calhoun, V., “Detection of mild traumatic brain injury by machine learning classification using resting state functional network connectivity and fractional anisotropy,” *J Neurotrauma* **34**(5), 1045-1053 (Mar 2017).
- [38] Aribisala, B.S., Cowie, C.J.A., He, J., Wood, J., Mendelow, A.D., Mitchell, P., and Blamire, A.M., “Multi-parametric classification of traumatic brain injury patients using automatic analysis of quantitative MRI scans,” *MIAR Medical Imaging and Augmented Reality* **2010**, 51-59 (2010).
- [39] Fedorov, A., Beichel, R., Kalpathy-Cramer, J., Finet, J., Fillion-Robin, J.C., Pujol, S., Bauer, C., Jennings, D., Fennessy, F., Sonka, M., Buatti, J., Aylward, S.R., Miller, J.V., Pieper, S., and Kikinis, R., “3D Slicer as an image computing platform for the quantitative imaging network,” *Magnetic Resonance Imaging* **30**(9), 1323-1341 (Nov 2012).
- [40] Sivic, J., and Zisserman, A., “Video Google: A text retrieval approach to object matching in videos,” *Conf Proc IEEE Int Conf Computer Vision* **2**, 1470-1477 (2003).
- [41] Krizhevsky, A., Sutskever, I., and Hinton, G., “ImageNet classification with deep convolutional neural networks,” *Advances in Neural Information Processing Systems* **25**, 1097-1105 (2012).

- [42] Russakovsky, O.,* Deng, J.,* Su, H., Krause, J., Satheesh, S., Ma, S., Huang, Z., Karpathy, A., Khosla, A., Bernstein, M., Berg, A.C., Fei-Fei, L., "ImageNet large scale visual recognition challenge," *Int J Computer Vision* **115**(3), 211-252 (Dec 2015).
- [43] Epstein, C., Carlsson, G., and Edelsbrunner, H., "Topological data analysis," *Inverse Problems* **27**(12), 120201 (2011).
- [44] Lum, P.Y., Singh, G., Lehman, A., Ishkanov, T., Veidemo-Johansson, M., Alagappan, M., Carlsson, J., and Carlsson, G., "Extracting insights from the shape of complex data using topology," *Scientific Reports* **3**, 1236 (Feb 2013).
- [45] Carlsson, G., "Topology and data," *Bull Amer. Math. Soc.* **46**, 255-308 (2009).
- [46] MATLAB version 9.0, Natick, Massachusetts: The MathWorks Inc., 2016.
- [47] Vedaldi, A., and Fulkerson, B., "Vlfeat: an open and portable library of computer vision algorithms," *Conf Proc ACM Int Conf Multimedia* **2010**, 1469-1472 (2010).